Anal. Chem. **2006,** *78,* 2342−2351

Multi-technique Comparison of Immobilized and Hybridized Oligonucleotide Surface Density on Commercial Amine-Reactive Microarray Slides

Ping Gong, Gregory M. Harbers, and David W. Grainger*

Department of Chemistry, Colorado State University, Fort Collins, Colorado 80523-1872

To establish a quantitative, corroborative understanding of observed correlations between immobilized probe DNA density on microarray surfaces and target hybridization efficiency in biological samples, we have characterized amine-terminated, single-stranded DNA probes attached to amine-reactive commercial microarray slides and complementary DNA target hybridization using fluorescence imaging, X-ray photoelectron spectroscopy (XPS) and ^{32}P-radiometric assays. Importantly, we have reproduced DNA probe microarray immobilization densities in macroscopic spotted dimensions using high ionic strength, high-concentration DNA probe solutions to permit direct XPS surface analysis of DNA surface chemistry with good reliability and reproducibility. Target capture hybridization efficiency with complementary DNA exhibited an optimum value at intermediate DNA probe immobilization densities. The macroscopic array model provides a new platform for the study of DNA surface chemistry using highly sensitive, quantitative surface analytical techniques (e.g., XPS, ToF-SIMS). Sensitive ^{32}P-DNA radiometric density measurements were calibrated with more routine XPS DNA signals, facilitating future routine DNA density determinations without the use of a hazardous radioactive assay. The objective is to provide new insight into different surface chemistry influences on immobilized DNA probe environments that affect target capture efficiency from solution to improve microarray assay performance.

Microarray technology is evolving rapidly as a powerful tool for large-scale parallel analysis of genome sequences and gene expression in biological and biomedical research, currently representing a substantial, maturing scientific method and accompanying commercial industry.[1−8] The potential of microarray applications and related parallel technologies for gene expression measurements requires more extensive microarray performance validation.[9] Earlier studies have shown poor reproducibility, repeatability, and result correlations among different microarray methods, indicating significant challenges for the broad application of microarray assays across platforms or among labs.[10−13] Recent collaborative efforts among microarray laboratories have demonstrated the importance of the proper use of microarray technology, stressing the significance of standardizing operating protocols.[14−16] Although not yet optimal, these recent studies have pointed to a much more positive prospect for reliable technology in bioassay and disease diagnosis. Nonetheless, several quantitative analytical issues remain in microarray assays, including limited detection sensitivity from complex milieu, absolute abundance, coefficients of variation, and more fundamental insight into assay mechanisms and limitations. With one recent exception,[17] lack of FDA approval for all current microarray assays for clinical patient use is one

* To whom correspondence should be addressed. Phone: 970-491-6717. Fax: 970-491-1801. E-mail: david.grainger@colostate.edu.

(1) Ramsay, G. *Nat. Biotechnol.* **1998**, *16*, 40−44.
(2) Schena, M.; Heller, R. A.; Theriault, T. P.; Konrad, K.; Lachenmeier, E.; Davis, R. W. *Trends Biotechnol.* **1998**, *16*, 301−306.
(3) Sanchez-Carbayo, M.; Bornmann, W.; Cordon-Cardo, C. *Curr. Org. Chem.* **2000**, *4*, 945−971.
(4) Freeman, W. M.; Robertson, D. J.; Vrana, K. E. *BioTechniques* **2000**, *29*, 1042−1044, 1046, 1048−1055.
(5) van Hal, N. L. W.; Vorst, O.; van Houwelingen, A. M. M. L.; Kok, E. J.; Peijnenburg, A.; Aharoni, A.; van Tunen, A. J.; Keijer, J. *J. Biotechnol.* **2000**, *78*, 271−280.
(6) Helmberg, A. *Exp. Gerontol.* **2001**, *36*, 1189−1198.
(7) Beaucage, S. L. *Curr. Med. Chem.* **2001**, *8*, 1213−1244.
(8) Yang, Y. H.; Speed, T. *Nat. Rev. Genet.* **2002**, *3*, 579−588.
(9) Sherlock, G. *Nat. Methods* **2005**, *2*, 329−330.
(10) Kuo, W. P.; Jenssen, T.-K.; Butte, A. J.; Ohno-Machado, L.; Kohane, I. S. *Bioinformatics* **2002**, *18*, 405−412.
(11) Ross, D. T.; Scherf, U.; Eisen, M. B.; Perou, C. M.; Rees, C.; Spellman, P.; Iyer, V.; Jeffrey, S. S.; Van de Rijn, M.; Waltham, M.; Pergamenschikov, A.; Lee, J. C.; Lashkari, D.; Shalon, D.; Myers, T. G.; Weinstein, J. N.; Botstein, D.; Brown, P. O. *Nat. Genet.* **2000**, *24*, 227−235.
(12) Tan, P. K.; Downey, T. J.; Spitznagel, E. L., Jr.; Xu, P.; Fu, D.; Dimitrov, D. S.; Lempicki, R. A.; Raaka, B. M.; Cam, M. C. *Nucleic Acids Res.* **2003**, *31*, 5676−5684.
(13) Yauk, C. L.; Berndt, M. L.; Williams, A.; Douglas, G. R. *Nucleic Acids Res.* **2004**, *32*, e124.
(14) Larkin, J. E.; Frank, B. C.; Gavras, H.; Sultana, R.; Quackenbush, J. *Nat. Methods* **2005**, *2*, 337−343.
(15) Irizarry, R. A.; Warren, D.; Spencer, F.; Kim, I. F.; Biswal, S.; Frank, B. C.; Gabrielson, E.; Garcia, J. G. N.; Geoghegan, J.; Germino, G.; Griffin, C.; Hilmer, S. C.; Hoffman, E.; Jedlicka, A. E.; Kawasaki, E.; Martinez-Murillo, F.; Morsberger, L.; Lee, H.; Petersen, D.; Quackenbush, J.; Scott, A.; Wilson, M.; Yang, Y.; Ye, S. Q.; Yu, W. *Nat. Methods* **2005**, *2*, 477.
(16) Bammler, T.; Beyer Richard, P.; Bhattacharya, S.; Boorman, G. A.; Boyles, A.; Bradford, B. U.; Bumgarner, R. E.; Bushel, P. R.; Chaturvedi, K.; Choi, D.; Cunningham, M. L.; Deng, S.; Dressman H. K.; Fannin, R. D.; Farin, F. M.; Freedman, J. H.; Fry, R. C.; Harper, A.; Humble, M. C.; Hurban, P.; Kavanagh, T. J.; Kaufmann, W. K.; Kerr, K, F.; Jing, L.; Lapidus, J. A.; Lasarev, M. R.; Li, J.; Li, Y.-J.; Lobenhofer, E. K.; Lu, X.; Malek, R. L.; Milton, S.; Nagalla, S. R.; O'Malley, J. P.; Palmer, V. S.; Pattee, P.; Paules, R. S.; Perou, C. M.; Phillips, K.; Qin, L.-X.; Qiu, Y.; Quigley, S. D.; Rodland, M.; Rusyn, I.; Samson, L. D.; Schwartz, D. A.; Shi, Y.; Shin, J.-L.; Sieber, S. O.; Slifer, S.; Speer, M. C.; Spencer, P. S.; Sproles, D. I.; Swenberg, J. A.; Suk, W. A.; Sullivan, R. C.; Tian, R.; Tennant, R. W.; Todd, S. A.; Tucker, C. J.; Van Houten, B.; Weis, B. K.; Xuan, S.; Zarbl, H. *Nat. Methods* **2005**, *2*, 351−356.
(17) http://www.roche-diagnostics.com/products_services/amplichip_cyp450.html (accessed Feb 2006).

10.1021/ac051812m CCC: $33.50 © 2006 American Chemical Society
Published on Web 02/25/2006

testament to the unsolved reliability and chemometric issues on this assay platform.

Extensive efforts have been directed to developing improved functional microarray surfaces using a broad range of surface chemistries. Surface chemistry serves as the foundation of microarray construction, significantly impacting important performance parameters, such as reproducibility, stability and availability of the immobilized biomolecules and nonspecific assay backgrounds that all affect assay signal-to-noise.[18] Sensing surfaces built on several model substrates, including gold, silicon, and glass, have been analyzed extensively. Quantitative, high-resolution, highly surface-sensitive techniques, including Fourier transform infrared spectroscopy (FTIR),[19,20] X-ray photoelectron spectroscopy (XPS),[19−23] secondary ion mass spectrometry (SIMS),[22,24−28] near edge X-ray absorption fine structure[29] and radiometric assays,[21,30−34] have provided data on both the properties of model sensing surfaces and immobilized biomolecular affinity capture components (antibodies, nucleotides) on surfaces, usually averaging surface spatial information across macroscopic features. However, these efforts for studying both individual and oligomeric nucleotides on various surfaces frequently do not directly address microarray technology in an assay-relevant context, especially with commercially available microarray surfaces and assay conditions. Additionally, many studies immobilize DNA to assay surfaces using bulk solution reactions that provide nucleotide immobilization dynamics, densities, and assay results distinct from commercial methods using microspotting in air in which nanoliter DNA solution droplets evaporate on the assay surface in seconds. Different immobilization densities resulting from these two immobilization conditions have profound implications for subsequent assay performance differences. Nonetheless, previous studies were able to show that XPS and SIMS are well-suited for sensitive characterization of surface-bound DNA. In particular, previous reports have identified unique nucleotide signals (nitrogen and phosphorus DNA-specific spectra) and demonstrated method utility in characterizing both composition and structure of DNA immobilized onto surfaces.[21,35−37] Applying highly surface-sensitive techniques directly to microscopic microarray features remains a challenge. Improved resolution may be obtained at the expense of higher sensitivity, and vice versa. Microarray feature sizes typically range from several tens to several hundreds of micrometers in diameter, making it difficult to achieve reasonable sensitivity along with suitable resolution for surface analysis.

No current single surface analytical method can accurately report absolute densities of microarrayed DNA on surfaces conveniently and consistently at high sensitivity. To facilitate improved microarray surface analysis in this context, we report macroscopic analogues of microarray spotted nucleotide features, allowing surface characterization without sacrificing sensitivity or resolution for widely used analytical techniques. Relevant to real-world microarray applications, immobilized DNA probe properties on commercially available microarraying polymer slides were compared using both microarray and macrospot formats. The primary motivation was to provide the first direct correlation between several surface analytical techniques for an important bioassay format (nucleotide microarrays) to remove the current molecular quantification limitations imposed by relative fluorescence intensity measurements characterizing these assays. First, comparable nucleotide probe immobilization efficiencies for both macro and micro spot sizes were demonstrated using fluorescence imaging with fluorescently labeled DNA probes. Immobilized probe and hybridized DNA target densities in macrospots were quantified using fluorescence, XPS, and ^{32}P-labeling and compared to fluorescence results from microarrays. DNA surface densities from these three methods showed very reasonable correlations. Sensitive ^{32}P-DNA radiometric measurements were calibrated with more routine XPS DNA P2p signals, facilitating future microarray immobilized DNA density determinations without the need to use the more hazardous radioactive assay.

EXPERIMENTAL SECTION

Materials. Phosphate, borate, and Tris buffer components; ethylenedicarbodiimide (EDC); *N*-hydroxysuccinimide (NHS); Tween 20; sarcosine; sodium citrate (SSC); sodium dodecyl sulfate (SDS); and ethanolamine were purchased from Sigma-Aldrich (St. Louis, MO) and used as received. Commercial polymer-coated microarray slides were purchased from Amersham (Codelink, Tempe, AZ). This microarray surface is marketed as an amine-reactive and three-dimensional (i.e., cross-linked polymer networks of thicknesses greater than a monolayer) hydrophilic polymer coating on low-fluorescence glass substrates. All slides were pretreated prior to probe immobilization to ensure optimum surface amine reactivity using an aqueous carbodiimide derivatization method previously described.[38]

Oligonucleotide Selection. DNA oligonucleotides were purchased from TriLink Biotechnologies (San Diego, CA); all oligo-

(18) Grainger, D. W.; Greef, C. H.; Gong, P.; Lochhead, M. J. In "*Microarrays: Methods and Protocols*" (*Methods in Molecular Biology*), 2nd ed.; Rampal, J. B., Ed.; Humana Press: Totowa, New Jersey, 2006, in press.
(19) Petrovykh, D. Y.; Kimura-Suda, H.; Whitman, L. J.; Tarlov, M. J. *J. Am. Chem. Soc.* **2003**, *125*, 5219−5226.
(20) Shen, G.; Anand, M. F. G.; Levicky, R. *Nucleic Acids Res.* **2004**, *32*, 5973−5980.
(21) Herne, T. M.; Tarlov, M. J. *J. Am. Chem. Soc.* **1997**, *119*, 8916−8920.
(22) Boland, T.; Ratner, B. D. *P. Natl. Acad. Sci.* **1995**, *92*, 5297−5301.
(23) Rabke, C. E.; Wenzler, L. A.; Beebe, T. P., Jr. *Scanning Microsc.* **1994**, *8*, 471−480.
(24) Patrick, J. S.; Cooks, R. G.; Pachuta, S. J. *Biol. Mass Spectrom.* **1994**, *23*, 653−659.
(25) Boland, T.; Ratner, B. D. *Langmuir* **1994**, *10*, 3845−3852.
(26) Benninghoven, A. *J. Vac. Sci. Technol., A* **1985**, *3*, 451−460.
(27) Arlinghaus, H. F.; Kwoka, M. N.; Jacobson, K. B. *Anal. Chem.* **1997**, *69*, 3747−3753.
(28) Arlinghaus, H. F.; Hoppener, C.; Drexler, J. *Secondary Ion Mass Spectrometry, SIMS XII*; Proceedings of the International Conference on Secondary Ion Mass Spectrometry; Brussels, Belgium, Sept. 5−10, 1999; , pp 951−954.
(29) Crain, J. N.; Kirakosian, A.; Lin, J. L.; Gu, Y.; Shah, R. R.; Abbott, N. L.; Himpsel, F. J. *J. Appl. Phys.* **2001**, *90*, 3291−3295.
(30) Cavic, B. A.; McGovern, M. E.; Nisman, R.; Thompson, M. *Analyst (Cambridge, U. K.)* **2001**, *126*, 485−490.
(31) Steel, A. B.; Levicky, R. L.; Herne, T. M.; Tarlov, M. J. *Biophys. J.* **2000**, *79*, 975−981.
(32) Zammatteo, N.; Jeanmart, L.; Hamels, S.; Courtois, S.; Louette, P.; Hevesi, L.; Remacle, J. *Anal. Biochem.* **2000**, *280*, 143−150.
(33) Balladur, V.; Theretz, A.; Mandrand, B. *J. Colloid Interface Sci.* **1997**, *194*, 408−418.
(34) Halliwell, C. M.; Cass, A. E. G. *Anal. Chem.* **2001**, *73*, 2476−2483.
(35) Petrovykh, D. Y.; Kimura-Suda, H.; Tarlov, M. J.; Whitman, L. J. *Langmuir* **2004**, *20*, 429−440.
(36) Samuel, N. T.; Castner, D. G. *Appl. Surf. Sci.* **2004**, *231−232*, 397−401.
(37) May, C. J.; Canavan, H. E.; Castner, D. G. *Anal. Chem.* **2004**, *76*, 1114−1122.
(38) Gong, P.; Grainger, D. W. *Surf. Sci.* **2004**, *570*, 67−77.

Table 1. Oligonucleotide Sequences and Modifications

		5′ modification	oligonucleotide sequence	3′ modification
A	Cy3-oligo1-NH_2	Cy3-	CTGAACGGTAGCATCTTGAC	$-C_6$-NH_2
B	Cy3-oligo1	Cy3-	CTGAACGGTAGCATCTTGAC	
C	NH_2-oligo1-^{32}P	NH_2-C_6-	CTGAACGGTAGCATCTTGAC	$-^{32}$P-dATP
D	oligo1-^{32}P		CTGAACGGTAGCATCTTGAC	$-^{32}$P-dATP
E	oligo2-^{32}P		GTCAAGATGCTACCGTTCAG	$-^{32}$P-dATP
F	oligo1-NH_2		CTGAACGGTAGCATCTTGAC	$-C_6$-NH_2
G	oligo2		GTCAAGATGCTACCGTTCAG	
H	Cy5-oligo2	Cy5-	GTCAAGATGCTACCGTTCAG	

nucleotides were HPLC-purified for highest purity.[39] The oligonucleotide sequence 5′-CTGAACGGTAGCATCTTGAC-3′ (oligo1) was selected because it forms a stable duplex with its complementary pair at room temperature, with minimal interference due to self-complementarity or secondary structure.[40,41] Table 1 lists all oligonucleotide sequences and modifications involved in this work. Oligos A and B were used in the fluorescence imaging section relating immobilized DNA microarray and macrospot densities; oligo A, for specific end-amine tethering, and oligo B, as a control for assessing nucleotide amine attachment and physisorption. Oligos C, D (as control of C and E), and E were used in radiometric assays for probe and target DNA density quantification. Oligos F and G were used for macrospot analysis with XPS. Oligo H was used for fluorescence analysis of DNA hybridization. In addition, oligos F and G were used as diluent DNA molecules in all fluorescence and radiometric assays.

Microarray Printing. Commercial polymer-coated amine-reactive slides (Amersham Codelink) were stored in vendor-sealed packaging per vendor recommendations until surface reactivity standardization using a previously described mthod.[38] Oligonucleotides containing a 5′-terminal hexylamine group were spotted onto microarray slides using a TeleChem SpotBot pin spotter and TeleChem SMP3-1 pins. Oligonucleotide solutions (Cy3-oligo1-NH_2 diluted 100-fold with oligo1-NH_2, Cy3-oligo1 diluted 100-fold by oligo1 to exclude dye self-quenching on printed surfaces) at spotting volumes of ~0.7 nanoliters (http://www.arrayit.com/Products/Printing/Stealth/stealth.html) were spotted in replicates of five at concentrations of 20, 10, 5, and 1 μM DNA in print buffer (150 mM PBS, pH 8.5 with 0.001% Tween20 and 0.001% sarcosine). These print conditions provided dried spots ~100−150 μm in diameter. Humidity was set at 50%. Stable surface immobilization was attempted by incubating the printed slides overnight at room temperature under 75% relative humidity.

Macrospot DNA Probe Immobilization. Probe DNA solutions (Cy3-oligo1-NH_2 diluted 100-fold with oligo1-NH_2 to exclude dye self-quenching on surface) at 50 μM concentrations were prepared in sodium phosphate buffer (pH 8.5) at concentrations ranging from 0.05 to 1.5 M to study the effects of ionic strength on immobilized DNA density. Adhesive silicone isolators (24-well, Grace Bio-Labs, Bend, OR) with 2.5-mm feature well diameters were applied onto substrate glass slides to define spotting areas. DNA solution (5 μL) was placed into each well and incubated at room temperature under 100% humidity for 3 h (XPS analysis showed little difference between bulk immobilization of DNA at 3 h and 22 h; data not shown). Replicates of at least three wells were randomly distributed on slides among the 24 wells.

For density quantification experiments, DNA solutions ranging from 1 μM to 400 μM were prepared in 1.0 M sodium phosphate buffer (pH 8.5) to produce immobilization commensurate with microspot oligoDNA print concentrations of 1−20 μM. The upper limit of 400 μM was restricted by practical limitations on reasonable amounts of DNA available. Adhesive silicone isolators (12-well, Grace Bio-Labs, Bend, OR) with 4.5-mm feature diameters were applied onto substrate glass slides to define spotting areas. DNA solution (10 μL) was added to each 4.5-mm well and incubated at room temperature under 100% humidity for 3 h. Replicates of at least three wells were randomly distributed on slides across 12 wells.

Postprint Array Treatment and Hybridization with Target DNA. Residual amine-reactive groups remaining on slides postprinting were consumed using blocking solution (50 mM ethanolamine in 0.1 M Tris, pH 9.0) at 50 °C for 30 min. Slides were then rinsed briefly with deionized water, then incubated in 4× saline−sodium citrate (SSC, 1× saline−sodium citrate solution contains 15 mM sodium citrate and 150 mM NaCl) containing 0.1% sodium dodecyl sulfate (SDS) for 30 min; rinsed again with deionized water; and finally, blown dry with nitrogen. Target hybridization was performed with commercial coverslips (1 ounce micro cover glasses, VWR, West Chester, PA) at room temperature under 100% humidity for 4 h in 4× SSC (with 0.1%SDS) solutions containing 1 μM DNA target. The solution ratio of Cy5-labeled DNA to identical nonlabeled DNA was 1:100. Slides were rinsed with 4× SSC (0.1% SDS) to remove the coverslips, followed by rinsing with 2× SSC/0.1%SDS for 5 min twice, then 0.2× SSC and 0.1× SSC, each for 1 min. Slides were finally blown dry with nitrogen.

Fluorescence Imaging. Microarray slides were scanned using a ScanArray Express Microarray Imager (Perkin-Elmer, Fremont, CA). Laser power and PMT sensitivity were set to 90% and 75%, respectively, for probe immobilization measurements, and 90% and 50%, respectively, for hybridization measurements. When slides were scanned at different power settings as specified above, the collected relative fluorescence units were normalized to values at the specified powers. Scanning resolution was 10 μm for microarrays and 50 μm for macroscopic spot features. Scanner channels 1 and 2 corresponding to 543-nm and 633-nm irradiations, were selected for the Cy3-labeled and Cy5-labeled experiments, respectively.

(39) Lee, C.-Y.; Canavan, H. E.; Gamble, L. J.; Castner, D. G. *Langmuir* **2005**, *21*, 5134−5141.
(40) Mazzola, L. T.; Frank, C. W.; Fodor, S. P. A.; Mosher, C.; Lartius, R.; Henderson, E. *Biophys. J.* **1999**, *76*, 2922−2933.
(41) Forman, J. E.; Walton, I. D.; Stern, D.; Rava, R. P.; Trulson, M. O. *ACS Symposium Ser.* **1998**, *682*, 206−228.

Image Processing for Spot Fluorescence Intensity Normalization. The microarray scanned fluorescence images were processed with ScanAlyze software (written by Dr. M. Eisen, University of California−Berkeley, Berkeley, CA; see http://rana.lbl.gov/EisenSoftware.htm). Arrays were first gridded with circles according to printing parameters, that is, resolution of scanned images, location of spots, and their position in the array. Grid parameters such as spot size and array tilt can be further fine-tuned according to the array image. Position of individual grid elements (circles) can be manually adjusted to fit each print spot image if necessary. ScanAlyze separates the image into pixels either contained within the identified spot or those that are not. Any pixel through which the spot circle passes is defined as being within the spot. Any pixels not within the spot but within a square, centered at the spot center, with side lengths of two-times the print spot radius (default value of 20) are defined as background pixels for this spot, excluding pixels contained within another spot. Pixel data intensities were imported into Microsoft Excel where background intensities were subtracted from corresponding spot intensities. Spots with defects that could be visually identified were excluded from replicate averaging (no more than 1 out of 5 replicates). Pixel intensities from replicates of five (or four in the case of a defective spot) were averaged, and standard deviations were calculated.

X-ray Photoelectron Spectroscopy (XPS) of Spotted Surfaces. XPS surface analyses were performed on a Physical Electronics PE5800 ESCA/AES system equipped with a 7-mm monochromatic Al Kα X-ray source (1486.6 eV) and hemispherical analyzer. All spectra were collected using an aperture size of 800 μm (diameter) and a low-energy electron flood gun to minimize surface charging. To compensate for residual charging effects, high-resolution spectra were charge-referenced by setting the hydrocarbon peak to 285.0 eV. A 35° photoelectron takeoff angle, defined as the angle between the surface plane and the axis of the analyzer lens, was used for all spectra. At this angle, sampling depth averages ~4.6 nm.[42] Compositional survey scans were initially used to detect all elements present using a pass energy of 187.80 eV and a step size of 0.8 eV. Once elements were determined to be present, all composition data (C1s, O1s, N1s, Si2p, Na1s, Cl2p, Ca2p, and P2p) were collected using a pass energy of 117.40 eV with a step size of 0.25 eV. High-resolution spectra (Si2p, C1s, N1s, and O1s) were collected at a pass energy of 23.5 eV and a step size of 0.05 eV. For P2p analysis on the DNA samples, utility spectra were collected for either 25 min or until a S/N ratio of 50 was obtained, whichever came first. Data analysis was conducted with either Multipak software (Physical Electronics, Chanhassen, MN) (utility) or Spectral Data Processor (v. 2.3) (XPS International) (high-resolution spectra). For quantitation, high-resolution phosphorus P2p peak areas were integrated using both 100% Gaussian and 90% Gaussian/10% Lorentzian peak-fitting constraints (endpoint: minimized χ^2 residuals). Both methods produced results insignificantly different from each other. Only results from (100% Gaussian) peak fits are shown. All values reported for the analysis of utility P2p spectra are the mean of at least three independent measurements from three experiments. Values reported for composition and high-resolution spectra are the average of three spots from a single Codelink microarray slide to allow for easy comparison between modification steps and eliminate the effect of slide-to-slide variability.

^{32}P-Radiometric Assay of DNA Surface Density. Oligonucleotides were labeled with α-^{32}P-ddATP (Amersham Biosciences, Piscataway, NJ) in the presence of terminal transferase (Roche Diagnostics Corp., Indianapolis, IN) and purified with an oligo mini spin column (Roche Diagnostics Corp., Indianapolis, IN). Concentrations of ^{32}P-labeled oligonucleotides were measured with a TriCarb 1500 liquid scintillation analyzer for specific activity determinations. Samples were exposed to a storage phosphor imager (Amersham Biosciences, Piscataway, NJ) for surface radioactivity measurement after DNA immobilization and hybridization. Gray scale pixelated images of surface ^{32}P density were obtained using a STORM (Amersham Biosciences) scanner and analyzed using ImageQuant software (v. 5.1, Amersham Biosciences). Quantitation of sample DNA surface density using gray scale image analysis was performed by constructing calibration curves for each labeling reaction as described by Steel et al.[31] DNA surface density values were averaged from three individual experiments (three spots per experiment). Control experiments comprised combinations of nonaminated probe (oligo D) macrospots, and noncomplementary targets hybridized to probe surfaces were performed. Nonspecific probe and target binding control signals were subtracted from the total assay signals to yield both probe and target signal shown.

RESULTS AND DISCUSSION

Buffer Ionic Strength and Its Effect on DNA Immobilization Efficiency. DNA microarray fabrication on a commercial microarraying substrate involves dispensing of nanoliter drops of liquid onto solid surfaces using a robotic spotter at a typical microarray printing humidity of lower than 50%. The nanoliter drops of liquid evaporate within 2 or 3 s of residence at the surface without reaching equilibrium in terms of DNA-surface interactions, mass transfer, covalent reactions on surfaces, or constant ionic strength. This evaporation results in significantly increased ionic strength of the spotting buffer as well as increased DNA concentration, leading to superior DNA probe surface immobilization efficiency to the advantage of microarray printing. This evaporative processing produces distinct differences in immobilized DNA physical chemistry on these surfaces versus bulk solution coupling reactions between DNA and surfaces. Few studies have appreciated these differences; few techniques are amenable to discerning such differences. Therefore, to achieve comparable levels of immobilized DNA probe at the macroscopic level, substantially elevated buffer ionic strength and increased DNA concentration are necessary to create macrospots on commercial microarraying substrates.

Polyelectrolyte immobilization efficiency is generally known to change with varying ionic strength of the print buffer.[43] Specific salt identity and ionic strength have also been reported to play a role in thiolated DNA assembly on gold[44,45] Similar ionic strength effects were observed for amine-oligoDNAs immobilized on

(42) Ratner, B. D.; Castner, D. G. In *Surface Analysis − The Principal Techniques*; Vickerman, J. C., Ed.; John Wiley & Sons, Ltd.: New York, 1997.
(43) Zhang, Y.; Tirrell, M.; Mays, J. W. *Macromolecules* **1996**, *29*, 7299−7301.
(44) Petrovykh, D. Y.; Kimura-Suda, H.; Whitman, L. J.; Tarlov, M. J. *J. Am. Chem. Soc.* **2003**, *125*, 5219−5226.
(45) Castelino, K.; Kannan, B.; Majumdar, A. *Langmuir* **2005**, *21*, 1956−1961.

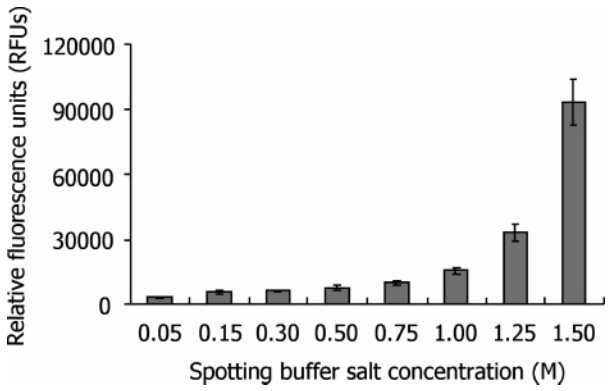

Figure 1. DNA probe immobilization dependence on buffer ionic strength studied using Cy3-labeled fluorescent DNA probes. Relative amounts of immobilized DNA probe molecules have been expressed as relative fluorescence units (RFU). A strong dependence of immobilization efficiency on media salt content was observed. By increasing buffer concentration from 0.15 to 1 M, the RFU signal from immobilized DNA probe increased ~3-fold; from 1 to 1.5 M, the signal amplification was 6-fold.

commercial polymer slides, shown specifically on macroscale DNA features using fluorescence labeling in Figure 1. Relative amounts of immobilized probe molecules are expressed as relative fluorescence units (RFUs). A strong dependence of immobilization efficiency on solution ionic strength was observed. By increasing immobilization buffer concentration from 0.15 to 1 M, relative amounts of immobilized DNA probe, as indicated by RFUs, increased ~3-fold, while increasing from 1 M to 1.5 M amplified the signal almost 6-fold.

Macrospot Analogue of Microspots Analyzed by Fluorescence Imaging (~4.5-mm Spot Diameter). Intensities of printed microarray spots (100−150 micron diameter) and bulk-immobilized macrospots (~4.5 mm diameter) were correlated using fluorescence imaging. In these fluorescent-labeled probe immobilization assays, Cy3-oligo1-NH_2 was diluted by oligo1-NH_2 (1:100), and Cy3-oligo1 was diluted by oligo1 (1:100) to exclude dye self-quenching, since without dilution (i.e., using 100% labeled probe) fluorescence signal plateaued at higher densities, presumably from fluorophore self-quenching. These probes were printed into microarrays and spotted as macrospot formats to compare amounts of total specific surface binding (Cy3-oligo1-NH_2) with nonspecific binding (Cy3-oligo1) resulting from either nucleotide base amine attachment[46] or physisorption. Because rapid evaporation eliminates equilibrium reactivity in microarray surface-immobilization reactions, this produces an immobilization endpoint and efficiency substantially greater than solution-phase immobilization reactions from bulk media, or "evaporation-free" equilibrium immobilization conditions. Hence, slowly drying macrodroplets in silicon gasket wells produces different immobilization DNA densities from rapidly evaporating microdrops under identical print conditions. Importantly, relative amounts of DNA probe immobilized onto slides under both microarray and macrospot formats can be directly correlated using fluorescently labeled DNA probes (Figure 2). Macroscale DNA immobilization using oligoDNA solution concentrations ranging from 1 to 400 μM (Figure 2A) produced immobilization yields commensurate with microspot

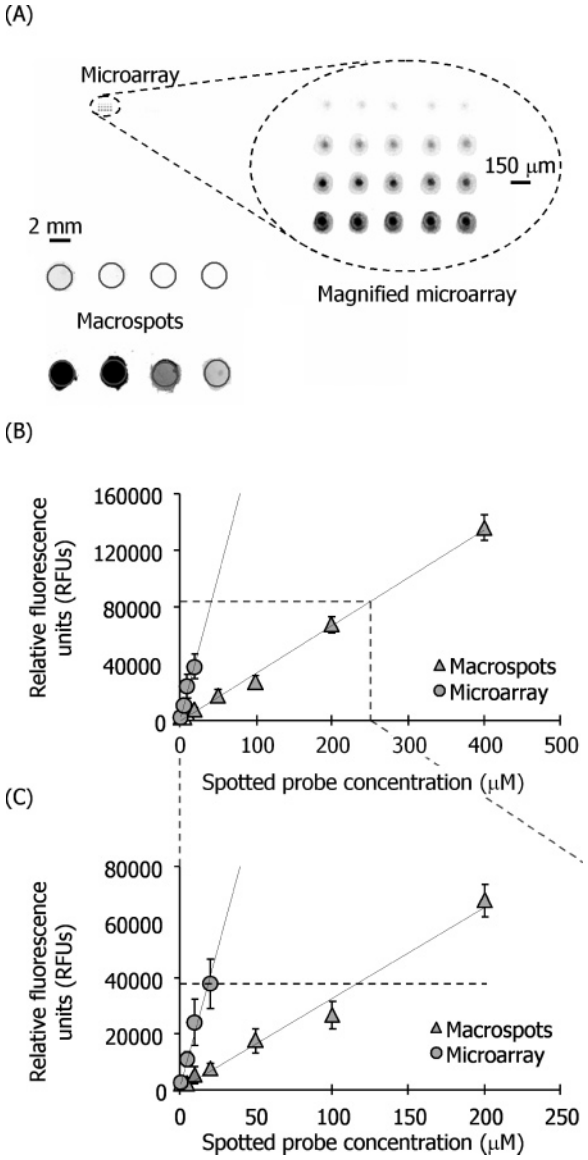

Figure 2. Relative amounts of DNA probe immobilized onto CodeLink slides are compared on microarray and macrospot formats using fluorescence-labeled DNA probes. (A) Macrospot array and microarray images are shown side by side. Microarrays are printed at four DNA concentrations (top to bottom rows: 1, 5, 10 and 20 μM, 150 mM sodium phosphate buffer, pH 8.5) in replicates of 5. Spotted macrospot (1.0 M sodium phosphate buffer, pH 8.5) concentrations are 1, 5, 10, 20 (upper row from right to left), 50, 100, 200 and 400 μM (lower row from right to left). (B) Macroscale DNA immobilization was studied using DNA solution concentrations ranging from 1 to 400 μM. A linear dependence of immobilized DNA density on applied solution DNA concentration was observed for both the micro- ($y = 2013.2x$, $R^2 = 0.9693$) and macro- ($y = 336.71x$, $R^2 = 0.9963$) spotting formats. (C) Resulting DNA probe density in a typical 20 μM microarray printing is equivalent to density from approximately 125 μM macroscale immobilization.

oligoDNA print concentrations of 1−20 μM. Throughout this concentration range, DNA probe immobilization efficiency exhibited a linear dependence on the concentrations of bulk probe solutions applied in both methods. As seen in Figure 2, the resulting DNA probe density in a typical 20 μM microarray printing is equivalent to the density achieved at ~125 μM macroscale solution immobilization (Figure 2B). Also worth noting

(46) Huang, E.; Zhou, F.; Deng, L. *Langmuir* **2000**, *16*, 3272−3280.

Table 2. XPS Elemental Composition Analysis of Modified Codelink Microarray Slides Used in DNA Macrospot Assays[a]

	atomic %							
slide surface	C1s	O1s	N1s	Si2p	Na1s	Cl2p	Ca2p	P2p
fresh, unmodified	53.1 (0.7)	25.7 (0.2)	10.3 (0.3)	7.5 (0.3)	2.9 (0.2)	0.3 (0.1)	0.2 (0.0)	nd
regenerated (see ref 38)	56.1 (1.8)	24.5 (0.9)	11.6 (0.3)	7.2 (0.6)	0.3 (0.0)	0.2 (0.1)	0.2 (0.1)	nd
blocked (ethanolamine)	53.2 (1.8)	26.5 (0.7)	11.2 (0.3)	8.2 (0.7)	0.8 (0.1)	nd	0.2 (0.0)	nd
DNA (200 μM) + blocking	52.5 (0.9)	26.6 (0.3)	12.3 (0.2)	7.2 (0.3)	0.8 (0.1)	nd	0.3 (0.1)	0.3 (0.1)

[a] To facilitate sequential stepwise surface modification comparisons, data were collected from a single slide (n = 3 spots; standard deviations shown in parentheses after each mean).

is the amount of nonspecific oligoDNA binding produced from either nucleotide base amine attachment or surface physisorption. In both microarray prints and macrospots, nonspecific DNA surface binding was negligible, in most cases <5% that of the specific end-amine tethering based on fluorescence analysis of total and nonspecific fractional DNA immobilization (data not shown). This indicates that lower nucleophilicity of nucleotide base primary amines is insufficient for reaction under these conditions, counter to a previous report.[46]

XPS Analysis of Surface-Immobilized and Hybridized DNA. DNA macrospots (4.5-mm diameter) on Codelink substrate chemistry were analyzed by XPS to compare each additional surface reaction (slide regeneration,[38] DNA immobilization, and NHS blocking) to the fresh, as received, microarray slides (Tables 2 and 3, and Figure 3). The slide polymer substrate chemistry has been reported elsewhere[47] and confirmed here by XPS to be consistent with polyacrylamide with activated ester groups providing attachment sites for aminated DNA. Compositional XPS data showed the presence of silicon, carbon, oxygen, nitrogen, and trace ions (calcium, sodium, and chlorine) within the polymer layer (Table 2). Compared to slides taken directly from vendor packaging, regenerated slides[38] showed increases in carbon and nitrogen signals and a decrease in oxygen and sodium. Carbon and nitrogen increased signal can be attributed to the reactivation of hydrolyzed carboxylic acid moieties to NHS active ester functional groups by regeneration,[38] and the modest decrease in oxygen is due to slight attenuation of the base glass substrate. With the addition of DNA, the most notable changes are the slight increase in nitrogen and the appearance of the P2p signal. A pure polyacrylamide layer has a theoretical C/N compositional ratio of ~3.3 and an analogous O/N of 1.0. The calculated C/N and O/N ratios of 5.1 and 2.5 from XPS results confirm the presence of additional chemical moieties (i.e., side chain DNA-reactive attachment sites on modified polymer) as well as the substrate signals and probable organosilane coupling layer and cross-linking agents. Substrate (glass) detection contributes to the increased oxygen signal, and a likely organosilane coupling layer facilitating attachment of reactive modified polyacrylamide to the base glass substrate, polymer active ester moieties, and cross-linking molecules all contribute to the increased C1s content consistent with the detected XPS atomic ratios. On the basis of the detection of the base silicon Si2p signal and given the XPS sampling depth of ~4.6 nm under these conditions, the overall average dry layer thickness of the Codelink polymer layer is apparently <5 nm to observe these signals.

In addition to the surface elemental composition data, high-resolution XPS data was collected for each of the adlayers (Table 3 and Figure 3). High-resolution XPS peak fits agree well with published data for polyacrylamide layers but deviate slightly due to the detection of the base substrate signal.[48] With the addition of the different surface reactions, the most notable changes in the high-resolution data are observed in the C1s data. Upon grafting of DNA, XPS hydrocarbon signal (285.0 eV) decreased (probable attenuation of the base substrate organosilane layer), and C−O/C−N content increased due to the presence of the overlayer of DNA bases. Changes within the Si2p, N1s, and O1s high-resolution peaks were only modest due to the overwhelming signal from the Codelink slide chemistry.

Substantial amounts of nitrogen (10−11 at. %) in the CodeLink polymer layer precluded efficient use of nitrogen for XPS study of DNA immobilization, leaving DNA phosphorus as the only unique characteristic element. Therefore, XPS quantification of relative amounts of surface-immobilized and hybridized DNA oligomers exploited this P2p signal. The intrinsically weak sensitivity of the phosphorus P2p signal combined with the resolution of this technique (spot size 800 μm) requires that a DNA feature be analyzed at the millimeter scale for meaningful signal analysis. Microarray-specific, on-spot analysis is, therefore, difficult without new, high-resolution imaging XPS capabilities.[49,50] Even with such imaging capabilities, reliable capture of meaningful nucleotide P2p XPS signals from micrometer-sized DNA features currently requires hours of data collection, significant XPS instrument time, and, hence, substantial resources. Hence, given current surface analytical instrumental limitations, an alternative to high-resolution imaging XPS of microarray DNA spots is the use of macroscale analogues of microarray spots compatible with conventional XPS resolution for microarray DNA density quantification. The same concept also applies to analyses of microarray DNA by other spatial resolution-limited techniques.

Therefore, XPS P2p spectra were collected for 4.5-mm-diameter macrospots immobilized at 0, 10, 50, 100 and 200 μM DNA probe concentrations, and then hybridized with 1 μM DNA target. For elemental comparisons of slides modified with different concentra-

(47) Ramakrishnan, R.; Dorris, D.; Lublinsky, A.; Nguyen, A.; Domanus, M.; Prokhorova, A.; Gieser, L.; Touma, E.; Lockner, R.; Tata, M.; Zhu, X.; Patterson, M.; Shippy, R.; Sendera, T. J.; Mazumder, A. *Nucleic Acids Res.* **2002**, *30*, e30/31−e30/12.

(48) Garg, D. H.; Lenk, W.; Berwald, S.; Lunkwitz, K.; Simon, F.; Eichhorn, K. J. *J. Appl. Polym. Sci.* **1996**, *60*, 2087−2104.

(49) Vohrer, U.; Blomfield, C.; Page, S.; Roberts, A. *Appl. Surf. Sci.* **2005**, *252*, 61−65.

(50) Blomfield, C. J. *J. Electron Spectrosc. Relat. Phenom.* **2005**, *143*, 241−249.

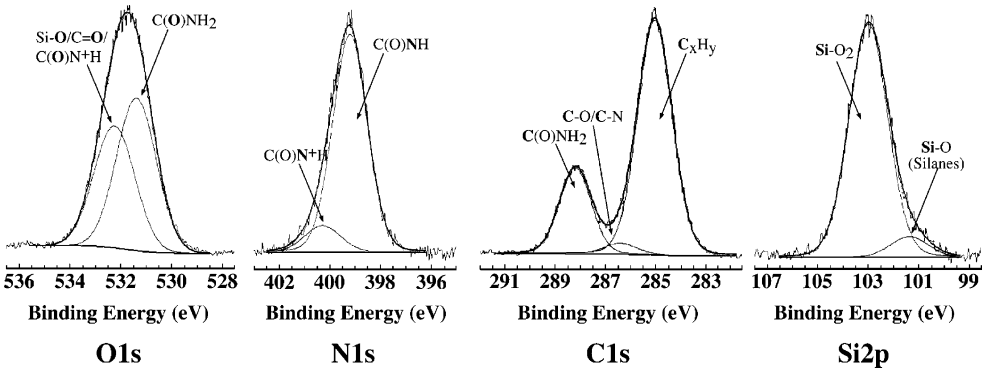

Figure 3. XPS high-resolution spectra for Si2p, C1s, N1s, and O1s signals for as-supplied Codelink microarray slides collected at a takeoff angle of 35° (sampling depth ~ 4.6 nm).

Table 3. High-Resolution XPS Chemical Species Analysis of Modified Codelink Microarray Slides[a]

			slide surface, %			
	eV		fresh	regenerated (see ref 38)	blocked	DNA[b]
Si2p	101.45 (0.01)	Si silanes	8.4 (0.4)	7.7 (1.8)	7.4 (1.2)	6.8 (1.2)
	103.07 (0.08)	Si in SiO_2	91.6 (0.4)	92.3 (1.8)	92.6 (1.2)	93.2 (1.2)
C1s	285.00 (0.00)	C_xH_y	72.6 (1.1)	72.0 (0.4)	71.9 (0.9)	66.7 (1.2)
	286.40 (0.00)	C−O/C−N	4.3 (1.2)	6.6 (1.0)	6.9 (1.0)	10.5 (0.4)
	288.20 (0.02)	$C(O)NH_2$	23.1 (1.0)	21.4 (1.0)	21.2 (0.6)	22.8 (0.8)
N1s	399.76 (0.03)	C(O)NH	90.9 (0.4)	96.8 (1.3)	97.0 (2.0)	95.2 (1.7)
	400.96 (0.01)	$C(O)N^+H$	9.1 (0.4)	3.2 (1.3)	3.0 (2.0)	4.8 (1.7)
O1s	531.45 (0.02)	$C(O)-NH_2$	59.2 (2.2)	52.9 (0.3)	55.6 (3.3)	55.7 (1.7)
	532.43 (0.09)	$Si-O/C=O/C(O)N^+H$	40.8 (2.2)	43.7 (1.2)	43.9 (3.1)	43.4 (0.1)
	533.78 (0.06)	C-O	nd	3.4 (1.4)	0.5 (0.4)	0.9 (1.2)

[a] To facilitate sequential stepwise surface modification comparisons, data were collected from a single slide (n=3 spots; standard deviations shown in parentheses after each mean). [b] For adlayer comparisons, DNA was coupled at 200 μM using the macrospot protocol; reported values are from DNA modified regenerated slides after blocking.

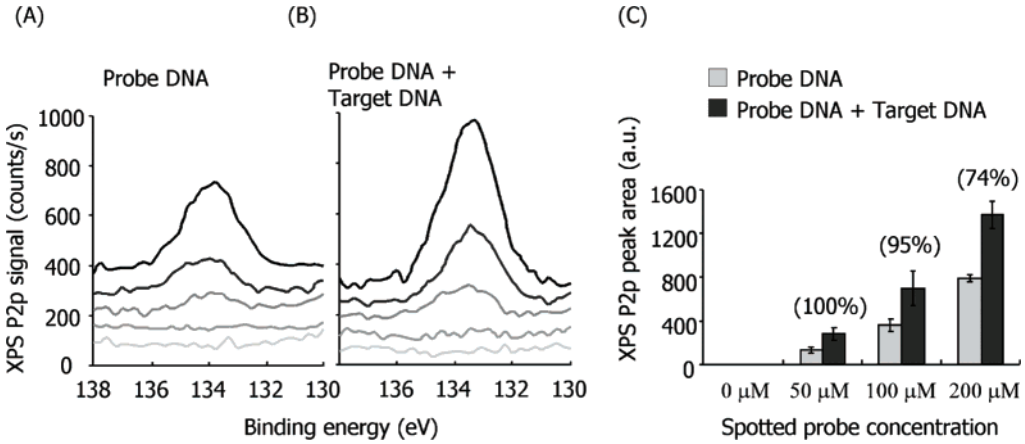

Figure 4. Relative amounts of surface-immobilized and hybridized DNA oligomers analyzed using XPS P2p signals. Amounts of DNA on CodeLink surfaces are proportional to integrated area underneath the characteristic phosphorus peaks. Integrated P2p peak area of the probe-immobilized (A) and target-hybridized (1 μM) (B) surfaces increased with increasing DNA probe solution concentration (200, 100, 50, 10, and 0 μM from top to bottom in figures). (C) XPS P2p peak areas were quantified, yielding hybridization efficiencies shown above each concentration (parentheses) derived as a percentage of probe molecules hybridized [((peak area of hybridized spot/peak area of probe spot) − 1) × 100%]. Hybridization efficiency slightly above 100% was rounded to 100%. Error bars represent results from at least three independent replicates.

tions of DNA, utility scans were collected for the main elements (Si2p, C1s, N1s, O1s, and P2p). The 0 μM DNA print control samples represent unmodified polymer slides exposed to identical buffer printing, incubation, postimmobilization wash and hybridization steps as the probe DNA-modified samples, but in the absence of DNA. Figure 4 shows the relative amount of surface-immobilized probe and hybridized DNA oligomers analyzed using XPS P2p peak integration. DNA surface amounts are proportional to the integrated area underneath the characteristic phosphorus peaks. The first high-resolution XPS P2p spectrum of surface-immobilized oligonucleotides on gold, collected and published by Tarlov et al.,[44] showed a single P2p peak observed at 133.6 eV in good agreement with the location of the P2p peak in single nucleotide species.[37] Integrated P2p peak areas have also been

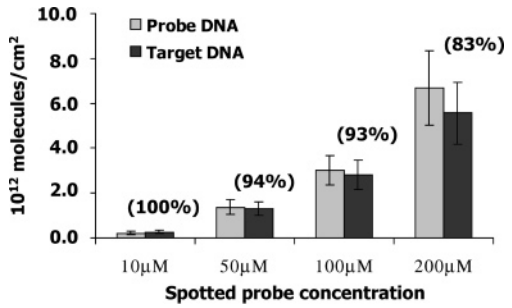

Figure 5. Absolute surface densities (molecules/cm^2) for DNA probe and target were quantified using radiometric methods. Hybridization efficiencies shown above each concentration (parentheses) were derived as percentage of probe molecules hybridized (target density/probe density × 100%). Hybridization efficiency slightly above 100% was rounded to 100%. Error bars represent results from at least three independent replicated experiments.

previously reported as a quantification method for immobilized DNA surface abundance on silane-modified silicon substrates when N1s cannot be used as a characteristic indicator of DNA.[20] With these precedents on model systems, we focused on creating an accurate surface quantification method that can be routinely applied to surface-bound DNA on commercial arraying substrates. To allow practical deployment for quality control, an XPS utility mode spectral acquisition with intermediate pass energy and step size was chosen instead of the more commonly used high-resolution mode to significantly shorten the sampling time while still maintaining satisfactory analytical spectral features. Both integrated P2p peak areas for probe-immobilized (Figure 4A) and target-hybridized (Figure 4B) surfaces increase with DNA probe solution concentration. Quantified peak integrated areas are shown in Figure 4C. Consistent with increasing P2p signal, XPS N1s signal also increased slightly, and Si2p (glass) signal decreased (data not shown), all consistent with DNA overlayer formation. Hybridization efficiencies were derived as a percentage of probe molecules hybridized [((peak area of hybridized spot/peak area of probe spot) − 1) × 100%]. Error bars represent results from three independent replicate experiments. A hybridization efficiency of 100% was obtained for the lower probe concentration samples (^{32}P density of the lower 10^{12} molecules/cm^2); at 200 μM probe print concentration, 70% hybridization efficiency was obtained. This lower hybridization efficiency at higher probe coverage can be explained by steric effects (molecular crowding): tethered polyanionic DNA probes closely packed by immobilization electrostatically repel and sterically hinder DNA targets from forming duplexes on the surface.[51−53]

^{32}P Radiometric Analysis of DNA Surface Density. Although XPS analysis provides element-specific, quantitative elemental information on relative amounts of DNA on the surface, it does not readily quantify absolute densities (e.g., molecules/cm^2). Absolute densities of immobilized DNA probes and hybridized DNA targets were quantified using ^{32}P end-labeled DNA. Density values shown in Figure 5 are the average of at least three independent experiments with three replicate spots per experiment. Consistent with fluorescence results, for all oligoDNA concentrations studied, a linear ^{32}P signal dependence was observed between immobilized probe density and spotted probe solution concentration for the macrospot method. Corroborating XPS results, ^{32}P-labeling results show that DNA surface probe density increased with increasing probe DNA concentration. Highest densities achieved using the 200 μM DNA probe solution in macrospot (nondrying) protocols were 6.7 × 10^{12} probes/cm^2. This density is limited by the amount of DNA practically available for immobilization (i.e., solution concentration and volume), not surface-activated, amine-reactive groups, because the dependence of immobilized probe density on spotting probe concentration did not reach surface saturation (e.g., no plateau was observed). Printed microarray oligoDNA probe density (desiccated nanodrops) at 20 μM DNA concentration, equaling RFUs from that of macrospotting at 125 μM DNA concentration (Figure 2), was extrapolated from ^{32}P data to be 4.1 × 10^{12} probes/cm^2. Hybridized DNA target density also increased with increasing printed probe DNA solution concentration, but hybridization efficiencies were higher at lower probe densities (e.g., 100% at 2.1 × 10^{11} probes/cm^2), decreasing slightly at densities of 1.4 × 10^{12} and 3.0 × 10^{12} probes/cm^2, and finally, diminishing to 83% at the highest oligoDNA probe density (6.7 × 10^{12} probes/cm^2). Calculated hybridization efficiencies slightly above 100% were rounded to 100%. Nonspecific protein binding, via base amine reaction[46] or by physisorption, may contribute to target hybridization signal detected. However, as control experiments indicate (subtracted in Figure 5), this contribution is <5% of the probe signal, therefore, much less than 5% of the total hybridization signal. This nonspecific contribution to assay signal is certainly a very minor component. Complete hybridization efficiency (e.g., 100% efficiency) dependence on probe density was in good agreement with values of (1.5−5) × 10^{12} probes/cm^2 reported by others immobilizing thiolated DNA on planar gold substrates from bulk solution adsorption.[21,54] The slightly lower values reported here could possibly be attributed to accessibility of probe DNA within the three-dimensional CodeLink gel matrix network compared to DNA−DNA duplex formation on planar gold surfaces.

Correlating XPS and Radiometric Results for DNA Surface Capture. To provide quantitative significance to relative fluorescence units shown in Figure 2, semiquantitative XPS results and quantitative ^{32}P-labeling results were integrated into correlative DNA signal calibration plots versus RFUs, shown in Figure 6(A−C). With these data, semiquantitative DNA surface density results collected from XPS can be calibrated against RFUs using absolute DNA surface densities obtained from radiometric ^{32}P labeling experiments. Results from the two quantitative approaches (Figure 6A) correlate linearly to high reliability (correlation coefficient > 0.99), providing a reliable standard curve useful for routine determinations of DNA surface densities using convenient lower resolution XPS analysis methods. This linear "standard curve" is empirical, with an intrinsic dependence on the surfaces, assay conditions, and DNA, but provides a conceptual basis to correlate multiple surface techniques in microarray validation. XPS and ^{32}P data were then further correlated with

(51) Heaton, R. J.; Georgiadis, R. M. (Trustees of Boston University, Boston, MA; Heaton, Jonathan R.). Application: WOWO, 2002, p 59.
(52) Peterson, A. W.; Heaton, R. J.; Georgiadis, R. M. *Nucleic Acids Res.* **2001**, *29*, 5163−5168.
(53) Heaton, R. J.; Peterson, A. W.; Georgiadis, R. M. *P. Natl. Acad. Sci.* **2001**, *98*, 3701−3704.
(54) Peterson, A. W.; Wolf, L. K.; Georgiadis, R. M. *J. Am. Chem. Soc.* **2002**, *124*, 14601−14607.

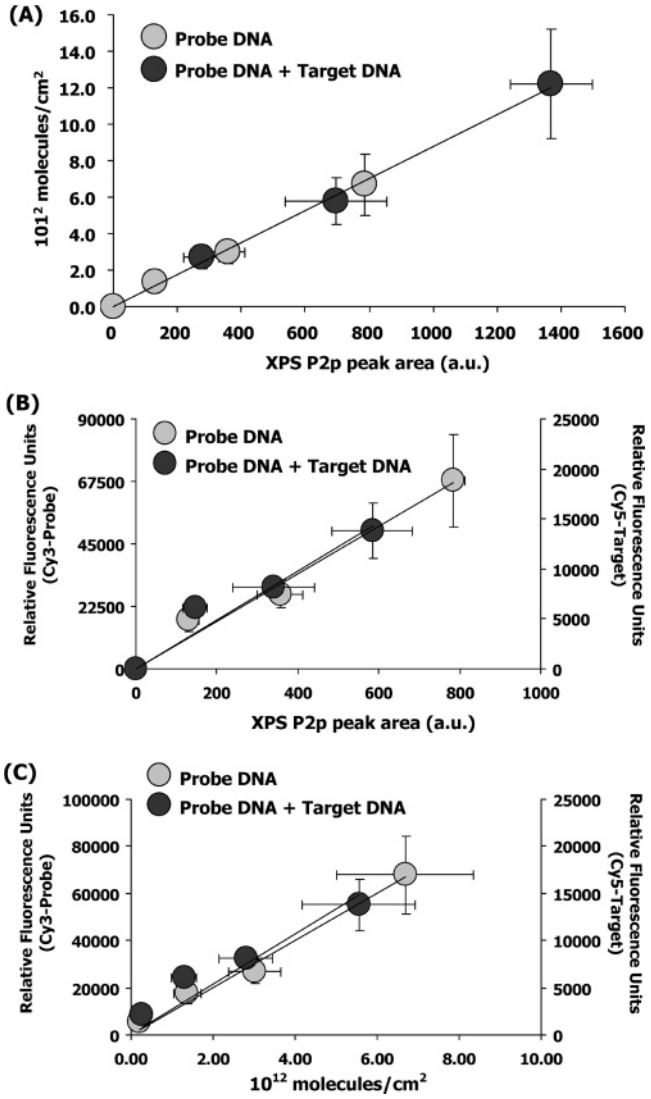

Figure 6. Cross-correlation of three different analytical methods for measuring DNA immobilization on commercial array slides: (A) Semiquantitative XPS P2p DNA surface density results (*x* axis) correlated to molecular ^{32}P-DNA surface densities (from radiometric labeling experiments) (*y* axis). Ordinary least squares regression produced a fit: $y = 0.0088x$ ($R^2 > 0.99$). (B) Cy3-DNA fluorescence probe (left) and Cy-5 DNA target (right) RFU signals correlated to XPS P2p DNA surface signals (lines are best-fit linear regressions for each data set). (C) Cy3-DNA fluorescence probe (left) and Cy-5 DNA target (right) RFU signals correlated to ^{32}P-DNA surface densities from radiometric labeling experiments (lines are best-fit linear regressions for each data set). In all plots, gray disks represent data points from surface immobilized DNA probe samples (right *y* axis); black disks represent data points from DNA hybridized samples (left *y* axis).

observed RFUs on identical arrays to apply DNA densities to array RFU signals. Figure 6B shows RFU signal relationships to XPS P2p signals for both immobilized probe and hybridized target on these surfaces. Linear correlations are observed between the data, suggesting that XPS P2p and RFUs are measuring similar DNA surface density profiles and that XPS validates RFU signals. Figure 6C makes this relationship quantitative, establishing a linear correlation between RFU signals for both immobilized probe and hybridized target signals on surfaces with DNA molecular density information from radioactive ^{32}P measurements. To our knowledge, this is the first such quantitative cross-correlation among conventional RFU measurements, XPS, and radiometric approaches to yield molecular meaning to both XPS and RFUs, especially on a commercial arraying platform.

In such correlations, we note that RFU intensities are largely case-specific and variable, depending significantly on the dye label chemistry and photophysics; the DNA labeling efficiency (i.e., batch-batch variations in labeled DNA probe or target from PCR); vendor methods for DNA labeling; and quite possibly, oligonucleotide sequence and length; and array substrate chemistry (unpublished observations). Additionally, scanning and image analysis conditions also provide an intrinsic source of RFU variation, in which different laser power PMT settings and collection optics from one scanner to another contribute to cross-platform RFU signal variation. A significant challenge in proving reliability and reproducibility for the bioanalytical metrics in microarray assays will be to establish a quantitative understanding of the common RFU unit; its standardization and interpretation in absolute molecular terms capable of absolute quantitation (compared to relative abundance); implications to microarray data interpretation; and, importantly, intrinsic limitations for applications in analyzing genetic assessments, disease diagnosis, and comparative expression assays.[9] We believe that this can currently be achieved by creating these cross-technique standard curves for nucleotide signals on surfaces and comparing information across these techniques.

CONCLUSIONS

Spotted, rapid-drying microarray DNA surface densities were successfully correlated with that of solution-phase macroscale immobilized DNA densities using XPS, fluorescence scanning, and radiometric methods. Fabrication of the 4.5-mm-diameter macroscale array analogues required significantly higher buffer ionic strength and probe DNA concentrations to provide immobilized DNA densities roughly equivalent to spotted, dried microarray formats. This was attributed to differences in DNA bulk solution applications to surfaces and nonequilibrium dynamics of rapid microspot solvent evaporation. Typical probe densities obtained in microarray printing, using 20 μM 20-mer aminated oligonucleotides in 0.15 M sodium phosphate spotting buffer, can be reproduced at macroscopic sizes using 125 μM DNA in 1 M spotting buffer. This DNA probe density was quantified using ^{32}P-radiometric assays to be 6.7×10^{12} probes/cm^2. Complete hybridization efficiency (100%) was achieved for lower DNA probe densities (e.g., at 10 μM probe concentration with resulting probe density of 2.1×10^{11} probes/cm^2). With increasing surface probe density, hybridization efficiency decreased slightly, maintaining a satisfactory efficiency of ~75−85% at the highest experimentally tested probe density of 6.7×10^{12} molecules/cm^2. The proven immobilization density equivalence of macroscale and microscale surface-immobilized DNA features allows molecular-level surface analysis by various quantitative, high-resolution surface analytical techniques that currently require features larger than a few hundred micrometers, such as XPS and FTIR methods.

Sensitive ^{32}P-DNA radiometric measurements accurately calibrate the DNA molecular densities from more routine XPS DNA analysis data, producing reproducible conversion of XPS signals into DNA molecular densities. This cross-comparison allows direct translation of high-resolution macro-scale DNA surface analysis

to microspot arrays, in which DNA surface information is currently limited. Importantly, this also facilitates future routine DNA density determinations on this commercial arraying surface by use of routine methods (e.g., XPS) compared with standard curves, without the need for hazardous radioactive quantitation assays once standard curves for a given arraying surface are established. Ultimately, these quantitative aspects should be correlated to the often-reported fluorescence RFU signal unit for industry standard and clinically relevant microarray assays as a step toward standardizing, interpreting, and directly quantifying this relative surface signal in this bioassay format. Absolute DNA molecular capture efficiencies as an assay endpoint should, therefore, be possible, in contrast to the relative data capabilities currently limiting the utility of the microarray assay technique. Last, such an approach demonstrated here for popular commercial arraying format can be applied to any microarraying surface, using multitechnique comparisons via surface-specific standard curves.

ACKNOWLEDGMENT

The authors are grateful for financial support from NIH EB001473. Technical assistance in fluorescence scanning from Dr. W. H. Hanneman (CSU) and insightful discussions with C. Greef, M. Lochhead, D. Castner, L. Gamble, and C.-Y. Lee are gratefully acknowledged.

Received for review October 10, 2005. Accepted January 19, 2006.

AC051812M